Chemistry-process morphology control of porous micro-structures: a bottom-up acoustic optimization approach

Arnaud Duval, Minh Tan Hoang, Camille Perrot, Valérie Marcel, Guy Bonnet

Chemistry-process morphology control of porous micro-structures: a bottom-up acoustic optimization approach

A. Duval[1], M-T. Hoang[1-2], C. Perrot[2], V. Marcel[1], G. Bonnet[2]

1: Faurecia Interior Systems, Acoustic TechCenter, Z.I F. Sommer BP13, 08210 Mouzon
2: Université Paris-Est, Laboratoire MSME UMR 8208 CNRS, 5 bd Descartes, 77454 Marne-La-Vallée

Abstract: Using numerical homogenization techniques at microstructure scale, one can simulate the acoustic macro-behavior of open-cell or partially closed-cell polymeric foams, typically their absorption coefficient or transmission loss. This link is realized through the scaling of an idealized 3D Periodic Unit Cell (PUC), which represents statistically the pores shape as regular arrays of polyhedra. Based on two non-acoustic standard measurements, namely the porosity and the static viscous permeability, plus a microstructure ligament length measurement as well as solid film thickness, the 3D PUC is scaled including membranes interconnecting the pores in the actual foam morphology. The opening of these membranes, constituting partially closed windows or throats between pores, proves to be an essential microstructure optimization parameter for sound absorption and mechanical behavior. On this 3D PUC, finite element computations are carried out in order to determine the intrinsic Biot-Allard parameters of the foam, by solving asymptotically the viscous Navier-Stokes flow at low frequencies, the inertial Laplace potential flow at high frequencies, the thermal conduction at low frequencies, as well as mechanical virtual pure tensile and pure shear strain tests. This micro-macro procedure proves to give good correlation with complete non-acoustic and acoustic characterization measurements, building a new reliable optimization scheme for poroelastic foams, which will be illustrated on a polyurethane injected soft foam.

Keywords: Porous media simulation, multi-scale modeling, micro-macro bottom-up approach

1. Introduction

With the recent generation of vehicles in the automotive industry, an overall – 25 % to – 30 % weight reduction on the NVH package has been reached through a “Kaizen” approach of existing foams, felts, barriers or non-woven technology optimizations, leading to a typical - 100 kg globally in the car (-10%). For the NVH noise treatments weighting between 25 kg and 60 kg typically, an auto-adaptative smart insulation / absorption combination on a single part depending on the pass-through quality situation allowed this first step [1].

Another – 25% weight reduction of the NVH package is underway for the next vehicle generation, with a deeper and better integration of the noise treatments in their environment (like an Instrument Panel optimal masking or even airtight closure), as well as clever overlapping and acoustic performance addition of insulators considered usually separately like the dash and carpet insulators or outer and inner dash insulators etc… Another improvement lever consists in switching from an acoustic insulating behavior to an absorbing one on a single insulator at different specific areas depending on their localization in the vehicle. These insulation, absorption or damping local properties balance tuning can be realized through for example a foil presence or an airtight hybrid foam-felt layer presence behind a stiff textile or fiber felt ([2], [3]). This will result in a weight reduction helping the global effort towards – 200 kg, but never towards – 300 kg which is necessary for the 2020 CO_2 EU emissions targets of 95 g CO_2 / km (instead of 130 g /km today on average).

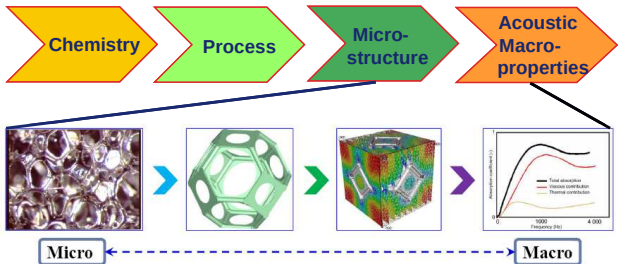

Figure 1: Bottom-up approach for microstructure optimization of sound absorbing materials

This last weight reduction step of an about – 25 % on the NVH package will only be possible through major architectural changes as well as material changes for both structural and NVH materials. This means that the foams, felts and non-wovens themselves will have to be drastically improved on all their sound absorbing, insulating as well as damping properties. A much better understanding of the intrinsic physical characteristics of poroelastic materials are therefore compulsory here. In order to tackle this issue, a bottom-up approach for microstructure optimization of sound absorbing materials will be described in this paper.

2. Microstructure morphology control of porous material: felts and foams

What is really at stake consists in linking the chemistry, the process, the corresponding microstructure and the resulting acoustic macro-parameters upwards and downwards (cf. Figure 1). Indeed, the ultimate goal would be from ideal Biot-Allard parameters (porosity, airflow resistivity, tortuosity etc…) determined by simulation to go downwards to the ideal microstructure and finally to the process and chemistry allowing manufacturing it.

This downwards path is not feasible for the moment unfortunately. It is necessary to work the other way around, in the bottom-up sense, the two last steps of Figure 1 being now established for 3D cases ([4], [5], [6]). In the absence of validated simulation tools to link the chemistry, the process and the resulting microstructures, one has to set-up experiences allowing to determine the influence of given product-process parameters on microstructure morphology changes [7].

This is typically the role that can be played by chemical formula components like cell opener, catalysts, water, surfactant (etc…) for a polyurethane foam for example. This bottom-up approach helps us determining what kind of cell morphology changes can be mastered from a chemistry-process perspective and how the acoustic macro-parameters will evolve accordingly using micro-macro numerical experiments (many at a time classically) [8]. One has then to choose the right cell morphology "morphing" answering the closest to his Biot-Allard parameters target.

2.1 Fibrous porous material case

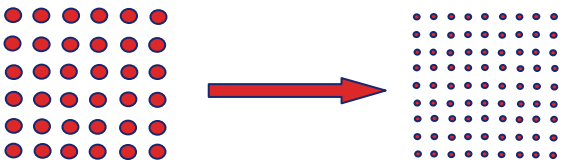

		PET felt homothetic reduction
Geometrical	Thickness (mm)	20
	Porosity Φ	→
	Thermal Characteristic Length Λ' (μm)	↘
Transport	Airflow Resistivity σ (N.m−4.s)	↗
	Tortuosity α∞	→
	Viscous Characteristic Length Λ (μm)	↘

Figure 2: Diameter size change of the fibers and compression rate: *homothetic reduction of the cell size*

The fibrous porous materials case is the simplest one, in the sense that the cell morphology is easy to control especially when using noble "sized controlled" fibers (diameter) and when adjusting the compression rate (throat size) for fibers that are laid horizontally in one direction (which one gets easily with carding/napping/thermofixing felt production processes, like PET felts). Typical fibers where one can control the diameter size are synthetic or mineral fibers like PET, PP, acrylic, glass fibers etc… All recycled felts, using cotton waste for example also called "shoddy", have to be analysed in a statistical fiber distribution sense on the contrary and present classically randomly oriented fibers (of about 2,5 dtex on average, which is too large) [9].

Figure 2 illustrates in 2D the optimization scheme for absorption properties that has been applied since 20 years using microfibers having diameters between 10 μm down to an ideal 1 μm (approximately 1 dtex down to 0,1 dtex for PET fibers) for either performance increase at identical mass per unit area (higher compression rate even at iso-thickness, also used for resistive screens) or weight reduction purposes of – 40 % to – 50% typically compared to "shoddy" (less compression rate: homothetic reduction).

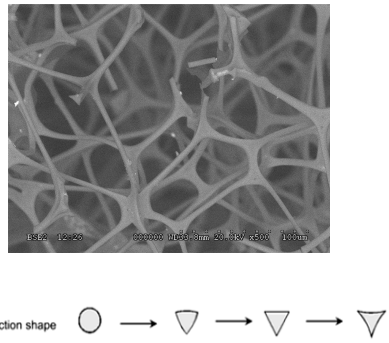

Figure 3: Cross-section shape morphology change: melamine foam "fiber like" case [8]

As illustrated Figure 3, another important cell morphology change lies in sculpting the cross-section shape down to a triangular concave one, which will at a given throat size, increase the porosity as well as increase the surface to volume ratio of the cell, meaning decrease the thermal characteristic length Λ'. The other parameters will follow the trend of Figure 2 in the case of a global homothetic reduction as well [8].

This is exactly what happens in the case of a melamine foam, which has a real "fiber like" microstructure with no membranes interconnecting the pores (and consequently almost no tortuosity), with typical ligament diameters of about 6 μm and small cell sizes compared to PUR foams with very low densities of 10 kg/m^3 typically. Apart from the pronounced triangular concave cross-section shape, the second difference of the melamine foam with a microfiber felt or felt in general (out of its high cost!) lies in its high stiffness, which restricts the melamine foam applications to absorption purposes only (or integrated in double wall air gaps without any

gluing). It is possible to manufacture felts or textiles with synthetic fibers having trilobal cross-section shapes, which are close to triangular ones, but only with too large diameters for the moment (3,3 dtex typically). These trilobal fibers are used today for their light refraction properties that improve the perceived quality and cleanability of a carpet for example.

2.2 Foam porous material case

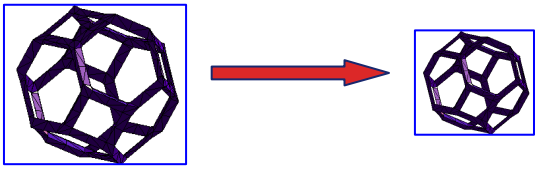

		Foam homothetic reduction
Geometrical	Thickness (mm)	20
	Porosity Φ	→
	Thermal Characteristic Length Λ' (µm)	↘
Transport	Airflow Resistivity σ (N.m–4.s)	↗
	Tortuosity α∞	→
	Viscous Characteristic Length Λ (µm)	↘

Figure 4: Diameter and length of the ligaments: *homothetic reduction of the cell size*

It is remarkable when observing systematically slab foams morphologies showing almost no membranes that the cell sizes are changing homothetically [10]. The macro-parameters will evolve roughly as summarized Figure 4, with almost constant porosities and tortuosities, which is very close to fiber felts indeed. Most of classical open porous PUR foams have rather large cells compared to melamine foams (or microfiber felts) with triangular cross-section shapes, while presenting low densities (15 kg/m^3) and high stiffnesses.

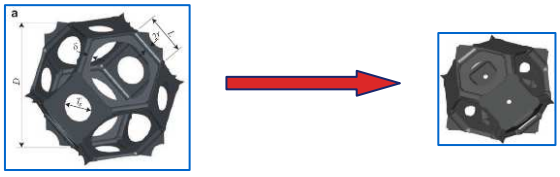

		Foam membrane closure
Geometrical	Thickness (mm)	20
	Porosity Φ	→
	Thermal Characteristic Length Λ' (µm)	↘
Transport	Airflow Resistivity σ (N.m–4.s)	↗↗
	Tortuosity α∞	↗↗
	Viscous Characteristic Length Λ (µm)	↘↘

Figure 5: Closure rate of the membranes: *homothetic reduction of the cell size*

This is also limiting such low density open porous PUR foams applications to absorption purposes only, while being significantly less absorptive than melamine foams or microfiber felts.

This was the status 15 to 10 years ago, the introduction of membranes interconnecting the pores as well as reducing the size of the PUR foam cells homothetically, as illustrated Figure 5, has eliminated the expensive melamine foams from the european engine compartments as well as endangered the position of glass microfiber felts (which have a good 6 µm fiber diameter though) thank to a significant weight reduction from 30 kg/m^3 down to 15 kg/m^3 or even 12 kg/m^3. As reported in [5] and summarized Figure 5, the introduction of membranes closing the foams have a very strong influence on the airflow resistivity as well as tortuosity increase, which is excellent for absorption properties in the middle frequency range (cf. Figure 6 afterwards). These very light slab foams remain very stiff and are very bad poroelastic decouplers behind heavy layers for insulation purposes.

3. Mechanical properties control of porous material

For the mechanical properties of the Periodic Unit Cell two main factors are driving the overall Young's modulus: the shape of the cell and the intrinsic Young's modulus of the constituting solid material: PUR, PET, glass, melamine etc… This last constituting material is mainly driving the damping loss factor as well. Some specific visco-elastic foam formulations present this way excellent damping loss factors of more than 0,41 (to be compared to 0,16 for standard elastic injected foam). Some specific "slick" treatments done on fibers may cause some extra friction effects that are increasing the mechanical damping of felts also and almost cancel the breathing frequency of a mass-spring system.

3.1 Fibrous porous material case

For insulator poroelastic springs applications behind heavy layers typically, the optimized PET or PET/PP microfiber felts, described section 2.1, are too soft and decouple badly in the middle frequency range. In order to reach the rather ideal softness of "shoddy" materials while reducing weight (E= 8 kPa typically), one may introduce spring crimped or helicoïdal hollow coarser fibers mixed with microfibers for improving the elastic properties, while keeping good visco-thermal dissipation properties [11]. On the contrary, glass fiber felts are too rigid for insulation purposes, due to a too high young's modulus of the constituting glass material itself (which can be tuned a little bit somehow with glass composition, but in a limited way), restricting applications to absorption purposes only or integrated in double wall air gaps without any gluing.

3.2 Foam porous material case

The influence of the foam cell morphology on its elastic properties will be discussed in section 6. Let us concentrate here on the stiffness control of foams realized through an adjustment of the young's modulus of the constituting material itself depending on the targeted absorption or insulation application in the PUR foam case. Regarding a specific PUR foam index situation, which depends on the mixing of diols and triols and therefore on the resulting available –OH radicals, as well as on MDI di-isocyanate molecule type with corresponding available N=C=O radicals, and while taking into account stoechiometric mixing ratios and water H_2O content, one can predict the number of "urethane" chemical bonds, which are directly linked to the stiffness of the foam (with "urea" secondary products bonds also). From this standpoint, it is then possible to scan above and below this stoechiometric value and get various soft Young's modulus values here, with a certain chemically feasible delta (collapse etc…).

4. Microstructure target setting

One has to distinguish two classes of noise treatment problems: the absorption ones quantified by sound absorption coefficients (energy dissipation) and the insulation ones quantified by Transmission Losses (energy reflection).

4.1 Transfer Matrix Method: absorption problem

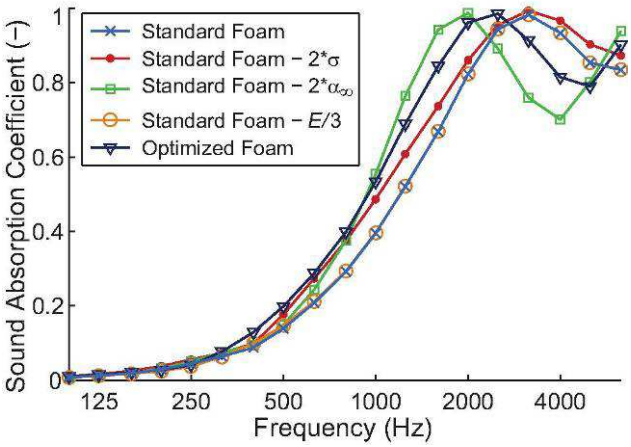

Figure 6: Absorption problem (TMM normal incidence): *Biot parameters target setting*

Using the classical Johnson-Champoux-Allard (JCA) 5 geometrical and transport Biot parameters of a standard soft foam implemented in a Finite Transfer Matrix Method code (FTMM), one can run optimization numerical experiences, where only one Biot-Allard parameter moves at a time: multiply by 2 the airflow resistivity and the tortuosity and divide by 3 the Young's modulus [12].

The results shown Figure 6 emphasize the importance of both airflow resistivity and tortuosity for improving the absorption in the middle frequency range particularly, even if the tortuosity should not exceed α_∞=2 in order to avoid too much absorption losses in the high frequency range. On the contrary, the Young's modulus divided by 3 decrease does not bring anything in this already soft foam absorption case (the frame is not excited here anyway).

4.2 Finite Transfer Matrix Method: insulation problem

For the insulation problem, a mass-spring system is considered, namely a heavy layer and the same standard soft foam, in order to excite both interstitial fluid and frame solid phases of this spring poroelastic foam.

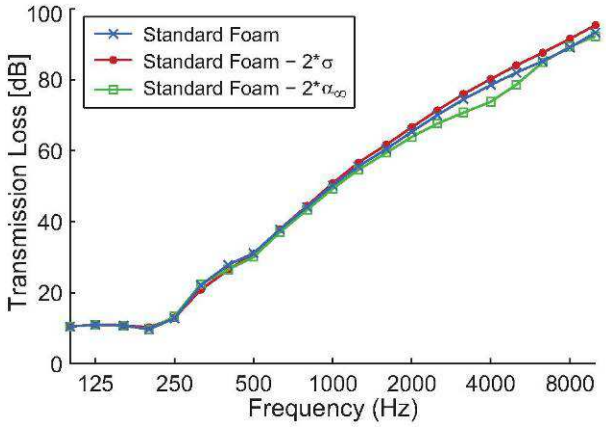

Figure 7: Insulation problem (FTMM diffuse field): *Biot parameters target setting*

The same FTMM numerical experiences are launched as for the pure absorption case (more refined systematic optimization analysis can be carried out with poroelastic finite elements like in [13]). Figure 7 shows the results for the same geometrical and transport Biot-Allard parameters, showing once again the importance of good airflow resistivity for improving the Transmission Loss by 1 dB to 2 dB above 1 kHz up to 10 kHz.

On the contrary, the tortuosity has a negative impact in the same high frequency area (without any gain in the middle frequency), which is directly linked to the drop in dissipation observed on its absorption coefficient of Figure 6 at 4 kHz as well.

Reducing drastically the Young's modulus alone brings a 1 dB improvement in the middle frequency range for the Transmission Loss between 500 Hz and 1 kHz (cf. Figure 8). The observed loss between 250 Hz and 500 Hz is linked to the quarter wave resonance of the first frame-borne Biot wave for the standard foam, which is often not observed with this magnitude experimentally [14].

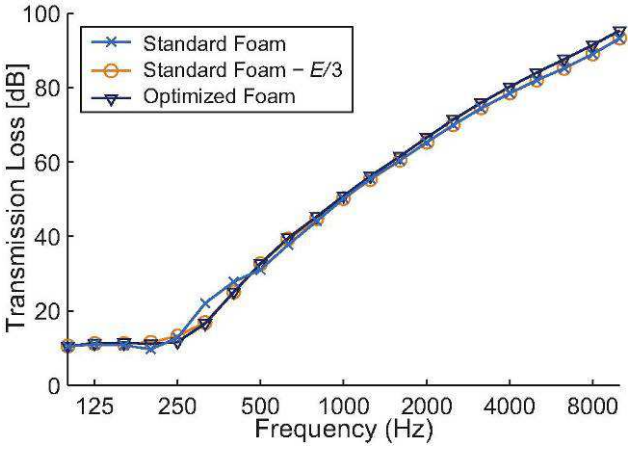

Figure 8: Insulation problem (FTMM diffuse field): *Biot parameters target setting*

Anyway, dividing by 3 the Young's modulus makes this resonance disappear, like we observe for very soft porous materials like felts. In the latter case, the complete poroelastic Biot-Allard model is not necessary anymore and the limp model is then sufficient [12]. The best optimized foam is then a combination of a doubled airflow resistivity and of a divided by 3 Young's modulus very soft spring foam, showing a 1,5 dB to 2 dB improvement in Transmission Loss from 500 Hz up to 10 kHz.

5. Micro-Macro approach: linking microstructure with acoustic macro-parameters

Figure 9 describes the hybrid "asymptotic FEM calculations" based procedure for simulating the acoustic macro-properties from a representative 3D PUC by using semi-phenomenological porous material models with thus identified Biot-Allard parameters for the computation of the dynamic equivalent density and the dynamic bulk modulus of foams. The great advantage of this hybrid method is the computational efficiency, by avoiding a computation at each frequency and by solving classical non-acoustic boundary value problems.

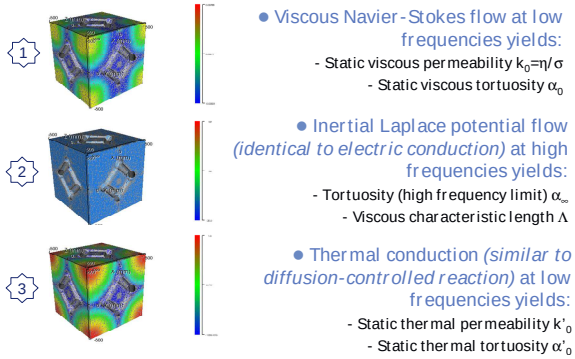

Figure 9: Macroscopic transport parameters are computed from three asymptotic calculations

The former FTMM target setting optimizing a soft poroelastic foam tends to lead to a homothetic cell size reduction morphology change (cf. section 2.2), which is expensive and critical mechanically because one has to rely on slab foams then (often too stiff) and not on injected foams classically. Reducing the cell size of injected PUR foams, as well as introducing much more closed membranes, seems to be the easiest way to reach the right high airflow resistivity, the low young's modulus (following section 3.2 methodology), as well as non wished "contained" tortuosity (α_∞<2 if possible) [7].

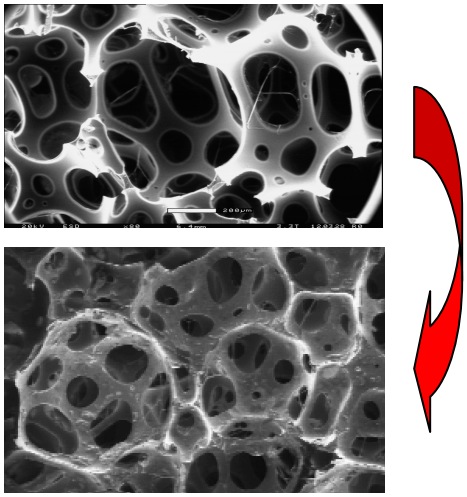

Figure 10: Microstructure morphology improvement: introducing more closed membranes in reduced cells (H1 lower foam) with *Scanning Electron Micrography*

Figure 10 illustrates this morphology switch from a typical open-cell rather coarse injected foam microstructure (above) to our optimized very soft H1 injected foam, with smaller pores and the presence of partially more closed membranes (below).

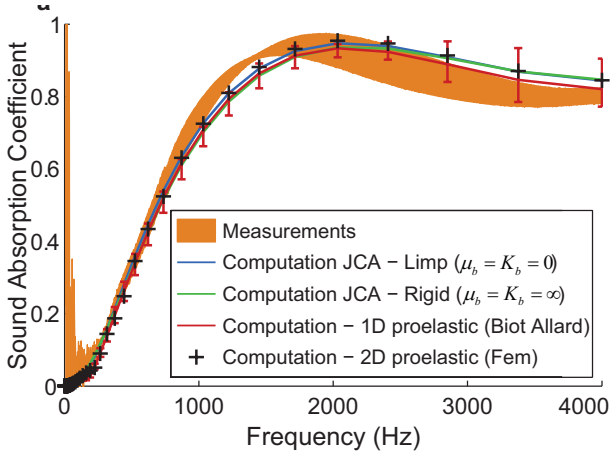

Figure 11: Normal incidence absorption coefficient 3D unit-cell TMM/FEM correlation: H1 foam

These micro-macro 3D unit-cell based computations can be correlated directly to the impedance tube absorption coefficient measurements (or Transmission Loss afterwards), as shown Figure 11 for the H1 foam with good results whatever the frame stiffness hypothesis may be here (rigid, limp or elastic for the Biot-Allard model). As expected for such a soft H1 foam, taking into account potential „bonded“ boundary conditions with an axisymmetric poroelastic 2D FEM code for the side of the sample doesn't change anything in the correlation quality (cf. Figure 11).

6. Linear elastic properties

The former FTMM Transmission Loss simulations show the importance of good mechanical properties for poroelastic springs optimizations. This section will describe briefly the methodology based on the homogenization of periodic media for obtaining the mechanical properties of the microstructure PUC, identified previously by pure sound wave propagation considerations in non-deformable porous media ([6], [15]).

Using voigt contracted notation and considering cubic symmetry, the elasticity equation reads when applying a uniform macroscopic tensile strain E_{11} to the unit cell:

$$\begin{pmatrix} \Sigma_{11} \\ \Sigma_{22} \\ \Sigma_{33} \\ \sqrt{2}\Sigma_{23} \\ \sqrt{2}\Sigma_{31} \\ \sqrt{2}\Sigma_{12} \end{pmatrix} = \begin{pmatrix} C_{11} & C_{12} & C_{12} & 0 & 0 & 0 \\ C_{12} & C_{11} & C_{12} & 0 & 0 & 0 \\ C_{12} & C_{12} & C_{11} & 0 & 0 & 0 \\ & & & C_{44} & 0 & 0 \\ & sym & & & C_{44} & 0 \\ & & & & & C_{44} \end{pmatrix} \begin{pmatrix} E_{11} \\ 0 \\ 0 \\ 0 \\ 0 \\ 0 \end{pmatrix} \quad (1)$$

Tensile strain

Cubic symmetry elastic matrix

Figure 12 illustrates the first FEM numerical experiment computation carried out at microstructure scale in order to get two elastic constants (equation (2)) from the macroscopic stress tensor.

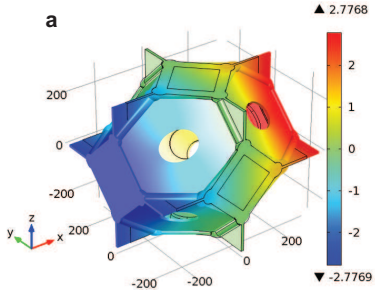

$$\begin{cases} C_{11} = \Sigma_{11}/E_{11} \\ C_{12} = \Sigma_{22}/E_{11} \end{cases} \quad (2)$$

Figure 12: Tensile strain numerical experiment: (a) displacement field (µm), (b) two elastic constants (2)

In the same way, the elasticity equation reads when applying a uniform macroscopic shear strain E_{12} to the unit cell:

$$\begin{pmatrix} \Sigma_{11} \\ \Sigma_{22} \\ \Sigma_{33} \\ \sqrt{2}\Sigma_{23} \\ \sqrt{2}\Sigma_{31} \\ \sqrt{2}\Sigma_{12} \end{pmatrix} = \begin{pmatrix} C_{11} & C_{12} & C_{12} & 0 & 0 & 0 \\ C_{12} & C_{11} & C_{12} & 0 & 0 & 0 \\ C_{12} & C_{12} & C_{11} & 0 & 0 & 0 \\ & & & C_{44} & 0 & 0 \\ & sym & & & C_{44} & 0 \\ & & & & & C_{44} \end{pmatrix} \begin{pmatrix} 0 \\ 0 \\ 0 \\ 0 \\ 0 \\ \sqrt{2}E_{12} \end{pmatrix} \quad (3)$$

Cubic symmetry elastic matrix

Shear strain

Figure 13 illustrates the second FEM numerical experiment computation carried out at microstructure scale in order to get the last elastic constant (equation (4)) from the macroscopic stress tensor in this cubic symmetry case.

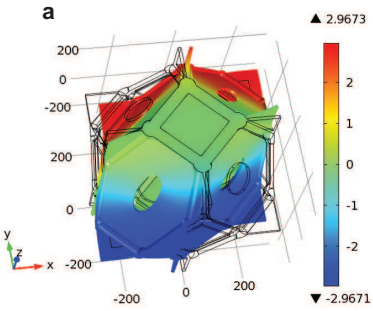

$$C_{44} = \Sigma_{12}/E_{12} \quad (4)$$

Figure 13: Shear strain numerical experiment: (a) displacement field (µm), (b) third elastic constant (4)

Eventually, the longitudinal elastic modulus and Poisson ratios definitions lead to ([6], [15]):

$$\begin{cases} E_L = \dfrac{C_{11}^2 + C_{11}C_{12} - 2C_{12}^2}{C_{11} + C_{12}} \\ \nu_{12} = \nu_{13} = \dfrac{C_{12}}{C_{11} + C_{12}} \end{cases} \quad (5)$$

The real challenge here lies in the determination of the microscopic Young's modulus of the skeleton of the foam here. For the H1 injected soft foam, the application of the Mercury Intrusion Porosimetry has led to the value E_μ= 7,07 ± 1.18 MPa, which is in line with our expectations of low values regarding to the formulation and foaming process parameters chosen.

The computed Young's modulus taking into account isotropic hypothesis and fixing the thickness of membranes to 1,7 µm obtained from SEM measurements (very influent parameter on the overall stiffness), gives E_{comp}= 59600 Pa for E_{exp} =14020 Pa measured by the Mariez-Langlois quasi-

static complex Young's modulus and Poisson ratio measurement device [13]. This first validation result gives the order of magnitude and is encouraging knowing the simplifications made on the geometry of the representative PUC.

Finally, the airflow resistivity (viscous permeability) and Young's modulus optimizations have led to a + 2 dB Insertion Loss improvement of the soft H1 foam as predicted Figure 8 and allow reaching the same TL performance as thermoplastic very soft felts with better damping properties. Nevertheless, a slight difference occurs between the H1 foam and the thermoplastic felt (called Trimelt by Faurecia) as poroelastic decoupler in the high frequency. The relatively high tortuosity of the foam leads to this slight TL decrease above 2,5 kHz compared to the thermoplastic felt, phenomenon which is perfectly caught by the FTMM simulation (cf. Figure 14).

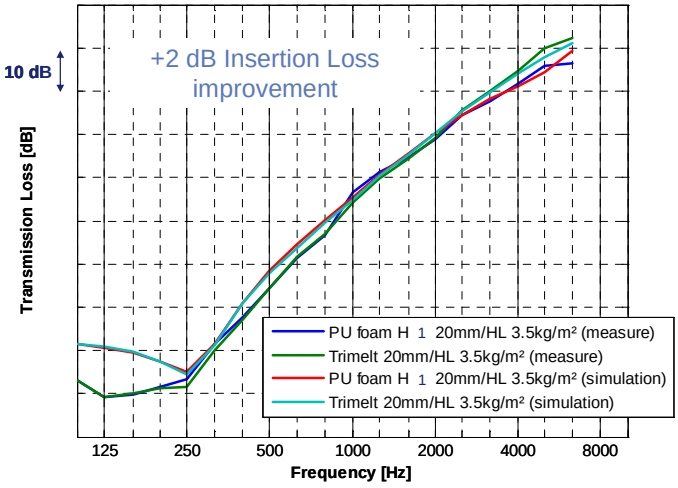

Figure 14: Diffuse field Transmission Loss 3D unit-cell FTMM correlation: H1 foam

5. Conclusion

This work shows the reliability and practicability of the bottom-up optimization approach illustrated here for not only "a posteriori" explanation purposes, but also for its powerfulness to actually drive optimization schemes for sound absorbing and insulating porous materials. Indeed, from only two standard non-acoustical measurements: the porosity and airflow resistivity (permeability), and two micrographic measurements: ligament length and membrane thickness, one can size the representative Periodic Unit Cell with membranes and compute with finite elements at this microstructure scale all Biot-Allard macro-parameters, including the elastic ones, with globally good correlations.

In the absence of chemistry-process simulation tools being able to predict the microstructure cell morphology for the moment, one can rely on a database of realistic morphology changes with associated Biot-Allard macro-parameters following various chemistry-process bottom-up scenarios. The ideal Biot-Allard intrinsic parameters targets determined using numerical optimization studies based on Transfer Matrix Method or poroelastic finite elements computations can thus be compared to "morphology feasible" set of parameters and lead to an optimal porous material choice, that one is actually able to manufacture.

The geometry of the tetrakaidecahedron with cylindrical ligaments and homogeneous thin membranes used as Periodic Unit Cell here remains simple and has to be progressively refined. The two first on-going improvements lie on a variable cross-section along the ligaments as well as various possible shapes like triangular concave ones (closer to observed foam microstructures classically). Another problem lies in the question whether a single PUC is able to catch the physics of rather irregular cell morphologies with abrupt changes in shapes and pore interconnections (throats). From a material development point of view, this last point seems to be an interesting one to follow, having observed already rather chaotic foaming processes in the presence of very small solid inclusions.

6. Acknowledgement

The authors would like to thank Jean-François Rondeau from Faurecia for the fruitful discussions during this work, as well as Fabien Chevillotte from Matelys for developing the software used in this study.

7. References

[1] A. Duval, J.-F Rondeau, L. Bischoff, G. Deshayes and L. Dejaeger, "Generalized Light-Weight Concepts: improving the acoustic performance of less than 2500 g/m² insulators" - 2009-01-2136, In SAE Conference, St Charles (IL), USA (2009).

[2] A. Duval, J.-F Rondeau, L. Dejaeger, F. Lhuillier and J. Monet-Descombey, "Generalized light-weight concepts: A new insulator 3D optimization procedure" - 2013-01-1947, In SAE Conference, Grand Rapids (MI), USA (2013).

[3] A. Duval and L. Bischoff: "Stiff textiles or felts glued on light impervious layers: a new "green" light septum fiber technology", SAPEM 2011, Ferrara, Italy (2011).

[4] C. Perrot, F. Chevillotte, M. T. Hoang, G. Bonnet, F.-X. Bécot, L. Gautron, and A. Duval, "Microstructure, transport, and acoustic properties of open-cell foam samples: Experiments and three-dimensional numerical simulations," J. Appl. Phys. **111**, 014911-16 (2012).

[5] M. T. Hoang and C. Perrot, "Solid films and transports in cellular foams," J. Appl. Phys. **112**, 054911-6 (2012).

[6] M. T. Hoang, G. Bonnet and C. Perrot, “Multi-scale acoustics of partially open cell poroelastic foams,” POMA 19, 065013-9 (2013).

[7] A. Duval, M. T. Hoang, V. Marcel, C. Perrot, “Development of acoustically effective foams: a new micro-macro optimization method”, in VDI Polyurethan 2012, Nürtingen, Germany (2012).

[8] C. Perrot, F. Chevillotte and R. Panneton, “Bottom-up approach for microstructure optimization of sound absorbing materials”, J. Acoust. Soc. Am., **124** (2), 940 (2008).

[9] J. Manning and R. Panneton, “Establishing relationships between acoustic and physical properties of shoddy-based fiber absorbers”, In Internoise 2009, Ottawa, Canada (2009).

[10] O. Doutres, N. Atalla, and K. Dong, “Effect on the microstructure closed pore content on the acoustic behavior of polyurethane foams”, J. Appl. Phys. **110**, 064901 (2011).

[11] A. Duval, F. Bonamy and R. Henry, FR2836748 B1 Patent Family “Mass-Spring Acoustic Insulation”, Faurecia, France (2002).

[12] J.-F. Allard and N. Atalla, *Propagation of sound in porous media: Modeling sound absorbing materials*, 2nd Ed., New York, Wiley (2009).

[13] L. Bischoff, Ch. Morgenstern, W. Berhard, A. Zopp and S. Schreck, "Replacement of damping pads by using soft visco-elastic foam while maintaining high insulation properties", In Internoise 2012, New York, USA (2012).

[14] A. Duval, L. Dejaeger, J. Baratier and J.-F. Rondeau: “Structureborne and airborne Insertion Loss simulation of trimmed curved and flat panels using Rayon-VTM-TL: implications for the 3D design of insulators”, In Congrès SIA Confort automobile et ferroviaire, Le Mans, France (2008).

[15] M. T. Hoang, G. Bonnet, H. T. Luu and C. Perrot: “Linear elastic properties from microstructures representative of transport parameters”, In Light-Weighting and Acoustical Materials in Vehicles SIA/SFA Conference, Compiègne, France (2013).

8. Glossary

PUC: Periodic Unit Cell

PUR foam: Polyurethane foam

NVH: Noise Vibration and Harshness

PET: Polyethylene terephthalate (polyester)

PP: Polypropylene

TL: Transmission Loss

HL: Heavy Layer

TMM: Transfer Matrix Method

FTMM: Finite Transfer Matrix Method

FEM: Finite Element Method

BEM: Boundary Element Method

dtex: Decitex, textile unit in g/10km of fiber

SEM: Scanning Electron Micrography